Supplementary Material for "Large enhancements in southern hemisphere satellite-observed trace gases due to the 2019/2020 Australian wildfires"

Richard J. Pope[1,2], Brian J. Kerridge[3,4], Richard Siddans[3,4], Barry G. Latter[3,4], Martyn P. Chipperfield[1,2], Stephen R. Arnold[1], Lucy J. Ventress[3,4], Matilda A. Pimlott[1], Ailish M. Graham[1], Diane S. Knappett[3,4] and Richard Rigby[1,5]

Supplementary Material (SM)-1: Satellite Observed Nitrogen Dioxide (NO_2)

We use tropospheric column NO_2 ($TCNO_2$) data from the TROPOspheric Monitoring Instrument (TROPOMI) on-board the ESA's Sentinel-5 Precursor (S5P) satellite (Veefkind et al., 2012). S5P was launched in October 2017 into a sun-synchronous polar orbit with a local overpass time of approximately 13.30. TROPOMI is a nadir-viewing instrument with spectral ranges of 270-500 nm (UV-Vis), 675-775 nm (near-infrared, NIR) and 2305-2385 nm (shortwave-infrared, SWIR). The TROPOMI retrievals represent the highest resolution of any current tropospheric trace gases sensor with a nadir horizontal resolution of 3.5 km × 7.0 km in the UV-Vis-NIR and 7.0 km × 7.0 km in the SWIR.

The response of $TCNO_2$ to the NDJ 2019/2020 Australian fires is less pronounced relative to the other trace gases investigated here due to the relatively short NO_2 lifetime of a few hours (Logan 1983; Alvarado et al., 2010). In December 2018 (**Figure S1a**), there are clear $TCNO_2$ hotspots (0.5-1.5 $\times 10^{15}$molecules/cm^2) in the north-western territories which clearly overlap with GFAS FRP (**Figure 1a** of the main manuscript). Similar relationships are seen near the coast in Queensland. Clear urban signals exist such as Sydney (over 4.0 $\times 10^{15}$ molecules/cm^2), Melbourne (over 4.0 $\times 10^{15}$ molecules/cm^2) and Brisbane/Adelaide (1.0-2.0 $\times 10^{15}$ molecules/cm^2). However, in December 2019 (**Figure S1b**), there was a large spatial increase in $TCNO_2$ values > 4.0 $\times 10^{15}$ molecules/cm^2 around Sydney. Again, these $TCNO_2$ hotspots are spatially correlated with fire activity (**Figure 1**) suggesting that fires have degraded the air quality in urban regions. **Figure S1c** shows the difference between December 2019 and 2018, where there are mixed $TCNO_2$ differences across the northern states, with enhancements (0.0-1.0 $\times 10^{15}$ molecules/cm^2) in the Western Australia territory and along the south-eastern coastline (2.0 $\times 10^{15}$ molecules/cm^2). To rule out other sources (e.g. urban) driving the $TCNO_2$ enhancement along the south-eastern coastline, $TCNO_2$ values have been weighted by FRP over the region (black box, **Figure S1c**) for the 2018/2019 (**Figure S1d**, red line) and 2019/2020 (**Figure S1d**, blue line). The FRP-weighted $TCNO_2$ signal for both seasons highlights sizeable variability, but 2019/2020 $TCNO_2$ values are larger in the first 20 days of November (3.0-6.0 $\times 10^{15}$ molecules/cm^2), peak in early December (>7.5 $\times 10^{15}$ molecules/cm^2) and remain larger for most of December. Overall, the time period average 2018/2019 and 2019/2020 FRP-weighted $TCNO_2$ values are approximately 2.2 $\times 10^{15}$ molecules/cm^2 and 3.3 $\times 10^{15}$ molecules/cm^2, respectively. To reduce the likelihood of this fire-$TCNO_2$ signal being dominated by other sources, **Figure S1e** shows time-series where the 2019/2020 $TCNO_2$ has been weighted by the 2018/2019 FRP and the 2018/2019 $TCNO_2$ has been weighted by the 2019/2020 FRP. The 2018/2019 $TCNO_2$ time-series (red lines in **Figures S1d & e**) are generally similar suggesting the NO_2 signal is not overly dependent on fire activity. However, in the 2019/2020 season (blue lines in **Figure S1e & d**), the time-series are substantially different where the 2019/2020 $TCNO_2$ series weighted by the 2018/2019 FRP is lower (0-3 $\times 10^{15}$ molecules/cm^2). Therefore, the large 2019/2020 $TCNO_2$ values are highly likely to be driven primarily by fire activity along the south-east coastline, especially around Sydney.

SM-2: Infrared and Microwave Sounding Extended Scheme

The original Infrared and Microwave Sounding (IMS) scheme was developed to retrieve water vapour, temperature and stratospheric ozone profiles from the Infrared Atmospheric Sounding Interferometer (IASI), Microwave Humidity Sounder (MHS) and Advanced Microwave Sounding Unit (AMSU) on the MetOp-A satellite (Siddans et al., 2015). This was used to produce a Version 1 data set from the MetOp-A mission 2007-16 (Siddans et al., 2018), which was delivered to the ESA Climate Change Initiative (http://cci.esa.int/watervapour).

The IMS scheme uses RTTOV as the radiative transfer model (forward model, FM). The optimal estimation method (OEM) is used to infer the atmosphere / surface state which best matches the observations, taking into account prior knowledge of the state. This is achieved by minimising the cost function:

$$\chi^2 = (\boldsymbol{y} - F(\boldsymbol{x}))^T \boldsymbol{S_y^{-1}} (\boldsymbol{y} - F(\boldsymbol{x})) + (\boldsymbol{a} - \boldsymbol{x})^T \boldsymbol{S_a^{-1}} (\boldsymbol{a} - \boldsymbol{x})$$

Equation 1

$\boldsymbol{y}$ is a vector containing each measurement used by the retrieval (a subset of all the channels available); $\boldsymbol{S_y}$ is a covariance matrix describing the errors on the measurements; $\boldsymbol{F(x)}$ represents the FM (RTTOV); $\boldsymbol{S_a}$ is the *a priori* error covariance matrix, which describes the assumed errors on the *a priori* estimate of the state, $\boldsymbol{a}$. The solution state which minimises the cost function is found via the Levenberg Marquardt approach (Rodgers, 2000), using the weighting function matrix, $\boldsymbol{K}$. This contains the derivatives of the measurements with respect to each element in the state vector (evaluated by the FM at a particular estimate of the state).

The IMS scheme has now been extended to retrieve tropospheric ozone, CO profiles and column amounts of additional trace gases, dust and volcanic sulphuric acid aerosol. Retrieval of those constituents benefit from accurate, co-located temperature, humidity and spectral emissivity which are co-retrieved by the IMS extended scheme. The IMS extension builds on new capabilities of RTTOV12 to model atmospheric scattering. Cloud and aerosol are modelled as scattering layers and each are retrieved in terms of an optical depth and layer height. Spectral absorption features of methanol, ammonia, formic acid, sulphur dioxide and nitric acid are optically thin. Therefore, these gases are retrieved by adopting a fixed reference profile shape for each and including in the state vector a scale factor for that profile with an extremely large *a priori* uncertainty. The reference profile for each gas is a constant i.e. height independent volume mixing ratio of 1 ppbv. The retrieved scale factors correspond, therefore, to column-averaged mixing ratios in ppbv which would pertain if the assumed flat profile shape was correct.

Most variables in the IMS extended state vector can be modelled directly by RTTOV12 (temperature, water vapour, ozone and carbon monoxide profiles, surface spectral emissivity and mass mixing ratio profiles of aerosol components). RTTOV12 can simulate variations in these quantities and returns the weighting functions needed for their optimal estimation. Although RTTOV12 does not explicitly model other minor gases, including methanol, it can compute the derivatives of simulated spectral radiances with respect to changes in the total absorption coefficient profile. Since their absorption features are optically thin, the radiance perturbation due to each gas can be calculated and added to the directly calculated RTTOV12 radiance as follows:

$$R'(\boldsymbol{x}) = R(\boldsymbol{x}) + x_{gas} \sum_{i=1}^{N} \frac{dR(x)}{dk_i} C_{gas} n_i$$

Equation 2

Where $R(\boldsymbol{x})$ is the RTTOV12 model simulation excluding minor gases. For a given gas in layer i of the N (=101) layers in the RTTOV12 model atmosphere, k_i is the (total) volume absorption coefficient (cm^{-1}), C_{gas} is the absorption cross section (cm^2); n_i is the number density (molecules cm^{-3}) at level i and x_{gas} is the scale factor for the gas (as included in state vector $\boldsymbol{x}$). Vertical sensitivity (e.g. air/surface temperature contrast, presence of cloud, optical thickness of other gases) is accounted for through the modelling of $\frac{dR(x)}{dk_i}$ by RTTOV12.

In total 119 IASI channels are used. Channels selected in the CO and methanol spectral ranges are indicated in **Figure S2a** and **b**. The measurement error covariance for IASI is assumed to be diagonal with variances as defined in the L1 file.

CO vertical profiles are retrieved in the extended IMS scheme in an analogous way to temperature, water vapour and ozone profiles in the original IMS scheme. Profiles are defined by the retrieval state vector (see below) on the 101 pressure levels on which the RTTOV12 coefficients for IASI are given. Surface temperature and surface emissivity are also defined by the state vector. Values for 2m temperature and 2m water vapour (also input parameters to RTTOV12) are defined by interpolating the profiles defined by the state vector. Surface pressure is defined from European Centre for Medium-Range Weather Forecasting (ECMWF) analysis (ERA-Interim) , adjusted to the mean altitude within the IASI footprint assuming the logarithm of the surface pressure varies linearly with the difference between the IASI altitude and that of the ECMWF model. This is the only parameter defined directly from NWP data in the IMS version 1 data.

The IMS state-vector ***x*** is defined such that there are no correlations between different retrieved product so corresponding off-diagonal elements in the prior covariance matrix are all zero.

Temperature (including surface temperature), water vapour, ozone and CO profiles are internally represented using basis functions, $\mathbf{M_x}$, which are the Eigenvectors of a covariance matrix which represents the prior variability of the profile on the 101 RTTOV pressure levels. 28 vectors are fitted for water vapour, 18 for water vapour, 10 for ozone and CO. Covariance matrices were computed using analyses for the three days 17 April, 17 July, 17 October 2013 from ECMWF for temperature and water vapour and the Copernicus Atmosphere Monitoring Service (CAMS) for ozone and CO. The zonal mean over all three days was computed and the covariance matrix used to define the state vector was calculated from the differences between all the individual profiles and their zonal mean. Global variability in CO during those days included that due to wild fires, the eigenvectors are therefore capable of representing plumes from such sources. The zonal mean and covariances were computed in K for temperature and ln(vmr) for water vapour, ozone and CO. The state vector comprises the coefficients of the Eigenvectors of the covariance matrix. Temperature profiles in (K) on the 101 RTTOV pressure levels are defined from the corresponding 28 elements of the state vector as follows:

$$\boldsymbol{T} = \boldsymbol{m_T}(\lambda) + \boldsymbol{M_T x_T}$$

Equation 3

Where $\boldsymbol{m_T}$ is the zonal mean (interpolated to the latitude of observation); $\boldsymbol{M_T}$ is the matrix of Eigenvectors and $\boldsymbol{x_T}$ the temperature sub-set of the state vector.

Water vapour, ozone profiles and CO (in ppmv) are defined similarly (now with exponent):

$$\boldsymbol{w} = e^{\boldsymbol{m_W}(\lambda)+\boldsymbol{M_W x_W}}$$

Equation 4

In terms of the state vector representation used in the OEM, the *a priori* state vector elements for temperature, water vapour, ozone and CO are all zero (the zonal mean profile is added in the FM). The prior covariance is diagonal with variances given by the Eigenvalues of the covariance matrix.

In order to speed up convergence, coefficients in the first guess state are estimated from ERA-Interim analyses using the above equations. Surface spectral emissivity is represented in the state-vector by a set of eigenvectors derived from the RTTOV emissivity atlas whose eigenvalues are co-retrieved with other variables (Siddans et al., 2015).

For column average CO, agreement with CAMS re-analysis in multi-year time-series is generally within ± ~10 ppbv (**Figure S3)**. Vertical sensitivity of the CO retrieval is illustrated in **Figure S4** which shows example averaging kernels as applied to the CAMS profiles for tropical land and mid-latitude sea.

In initial fits to IASI observations with the IMS extended scheme, systematic spectral residuals were found (below 2000 cm^{-1}) which are significant compared to the instrument noise. These are accounted for in the retrieval by fitting two "spectral residual patterns", vectors $\boldsymbol{b_0}$ and $\boldsymbol{b_1}$ which were derived by averaging the differences between observed and simulated spectra over sea in the latitude range 60°S to 60°N (for 3 selected days in each season). These simulations adopted ECMWF analyses for temperature and water vapour and CAMS analyses for ozone and assumed no methanol to be present. The difference spectra were analysed to obtain the mean residual spectrum ($\boldsymbol{b_0}$) and the spectrum of an additional component which varies linearly with off-nadir scan-angle ($\boldsymbol{b_1}$). These two fixed patterns were then added into the forward model for use in subsequent analyses:

$$F(\boldsymbol{x}) = R'(\boldsymbol{x}) - x_{b0}\boldsymbol{b_0} - x_{b1}\boldsymbol{b_1}$$

Equation 5

Where x_{b0} and x_{b1} are retrieved parameters (included in the state vector, with negligible prior constraint). Vectors $\boldsymbol{b_0}$ and $\boldsymbol{b_1}$ are both fixed to zero in the CO fit window.

From **Equation 2**, it is straightforward to derive weighting function profiles, $\boldsymbol{K_{gas}}$, for each minor gas (derivative of $F(\boldsymbol{x})$ with respect to the number density at each level). Example weighting functions for the methanol spectral feature at 1034cm^{-1} are shown in **Figure S5.**

It is important to note that infrared sensitivity to methanol varies greatly with height. Above the surface, the weighting function is negative because methanol absorbs radiation emitted from the warmer surface. However, sensitivity is low near to the ground due to the very small difference between the atmospheric temperature and that of the surface. If the surface temperature is lower than the atmospheric layer above, the methanol weighting function in that layer will be positive. Because the top-of-atmosphere spectral signature of methanol is strongly dependent on the temperature profile and surface-air temperature contrast, the shape of the methanol reference profile adopted in the fit is critical to the retrieved scale factor and hence column average mixing ratio. Adopting a constant mixing ratio with height as reference profile will result in a smaller column average being retrieved than would be the case if the reference profile contained more methanol near the surface. If methanol is assumed to be near the surface, where sensitivity is weak, then a larger amount is needed to explain a given observed spectral signature than would be the case if the methanol is assumed to be at a higher, colder altitude, where the sensitivity is stronger. In order to look at geographical and temporal variations consistently it is desirable to apply a retrieval scheme uniformly across the globe. Rather than tailor the shape of the reference profile according to expectations from an emission inventory, the flat profile shape has therefore been adopted everywhere. Over emission sources, however, methanol is usually located close to the surface, so it

is to be expected that this reference profile will lead to a lower column average being retrieved than a realistic model would predict. This can be accounted for in model comparisons by applying averaging kernels which characterise the sensitivity of the retrieved methanol column average to perturbations in the true methanol *profile*:

$$\boldsymbol{A_{gas}} = \boldsymbol{G_{x_{gas}}}\,\boldsymbol{K_{gas}}$$

Equation 6

Where the matrix $\boldsymbol{K_{gas}}$ contains the derivatives of the measurements with respect to methanol profile perturbations at each of the vertical levels in the FM and $\boldsymbol{G_{x_{gas}}}$ is the derivative of the retrieved methanol scale factor with respect to perturbations in the measurement vector. $\boldsymbol{G_{x_{gas}}}$ is one row of the retrieval gain matrix (containing the derivatives of each state vector element with respect to perturbations in each measurement), given by the standard equation (Rodgers, 2000):

$$\boldsymbol{G} = \langle \boldsymbol{K^t S_y^{-1} K} + \boldsymbol{S_a^{-1}} \rangle^{-1} \boldsymbol{K^t S_y^{-1}}$$

Equation 7

Where $\boldsymbol{K}$ is the weighting function matrix giving the derivative of the forward model with respect to all elements of the state vector (including the methanol scale factor). **Figure S5** shows that because $\boldsymbol{G_{x_{gas}}}$ is a vector (same dimension as the measurement vector), the methanol averaging kernel $\boldsymbol{A_{gas}}$ (dimension FM levels) has practically identical shape to the methanol weighting function, $\boldsymbol{K_{gas}}$ (though usually with reversed sign)**.** Magnitudes of the elements of $\boldsymbol{A_{gas}}$ depend on the assumed reference profile shape (because the elements of $\boldsymbol{K}$ corresponding to the methanol scale factor depend on the profile shape).

$\boldsymbol{A_{gas}}$ can be used to estimate the column amount, $\boldsymbol{x_{iso:m}}$, that the retrieval is expected to return given a model methanol concentration profile, $\boldsymbol{n_m}$:[1]

$$\boldsymbol{x_{meth:m}} = \boldsymbol{A_{gas}}\,\boldsymbol{n_m}$$

Equation 8

This accounts for the effects of varying vertical sensitivity and the profile shape assumed in the retrieval. Because the reference profile shape is implicit to $\boldsymbol{A_{gas}}$, changing that will change $\boldsymbol{x_{meth:m}}$ as well as the retrieved column average, but it will not change the relative agreement between the two. (Changing the assumed profile shape simply scales both quantities.)

The solution error covariance matrix for an optimal estimation retrieval is given by:

$$\boldsymbol{S_x} = \left(\boldsymbol{S_a^{-1}} + \boldsymbol{K^T S_y^{-1} K}\right)^{-1}$$

Equation 9

The estimated error on the retrieved methanol column average is given by the square-root of the diagonal element of $\boldsymbol{S_x}$ which corresponds to $\boldsymbol{x_{gas}}$.

The IMS extended scheme is applied to all scenes, irrespective of cloud, however the presence of extensive, thick cloud limits retrieval quality and of course no information on minor gases such as CO or methanol is available below optically thick cloud. A simple test is used here: the difference in brightness temperature between the IASI observed spectral radiance at 950 cm^{-1} and that simulated on the basis of temperature and humidity profiles and surface temperature interpolated from

[1] *The prior constraint for the retrieved methanol scale factor is negligible so can be neglected in Equation 8.*

ECMWF analyses is calculated. If this difference (observation – simulation) is outside the range of -5 to 15 K, the scene is flagged as cloudy. These scenes are not used at all in the analysis reported here.

The scheme applied here therefore differs in a number of key respects from that applied to global methanol retrieval from IASI reported by Razavi et al. (2011). Their scheme used brightness temperature differences between three channels near the methanol Q branch peak near 1034 cm^{-1} and six neighbouring channels where methanol absorption is low and conversions factors to methanol column derived from optimal estimation retrievals using online line-by-line modelling. Methanol is retrieved in four layers adopting a terrestrial and a marine profile as prior with variability from a chemical-transport model as covariance matrix diagonals and a long correlation length for off-diagonals. It is also radically different from the neural net scheme employed by Franco et al. (2018).

SM-3: Satellite Observed Methanol (CH_3OH)

Methanol (CH_3OH) infrared absorption features are much weaker than those of CO and background levels of CH_3OH over ocean outside fire plumes are too low to be detectable in individual soundings above IASI's level of noise-equivalent spectral radiance (NESR), so retrieved values there are zero ± NESR. At locations of temperature inversion, where methanol spectral features appear in emission above a baseline of colder surface emission, retrieved scaling factors for the methanol reference profile are negative (see SM-1). Systematic errors, due for example to insufficiently accurate handling of interference from neighbouring spectral lines, can also result in averaged CH_3OH being negative in these marine regions, though not significantly so in comparison to their estimated errors (see **SM-2**, **Figure S6).** The white region in **Figure S6** shows where we have filtered out retrievals with large errors (i.e. >15.0×10^{15} molecules/cm^2). In the multi-month average (November-December 2019, January 2020) there still appears to be a negative offset in the IASI retrievals. For this work, we subtracted a negative background value of -3.68 ×10^{15} molecules cm^{-2} from individual retrievals used in **Figure 4** and **Figure 5** of the main manuscript. This background value was based on data between the 1st and 17th January 2020 covering part of the North Pacific (135°E-115°W, 0-30°N).

Intercomparing the fire seasons (November-December-January, NDJ), IASI detects clear enhancements in $TCCH_3OH$ during 2019/2020. Over Australia and South America (**Figure S7a & c**), $TCCH_3OH$ ranges between 8.0-15.0 ×10^{15} molecules cm^{-2} and 6.0-10/0 ×10^{15} molecules cm^{-2}, in both NDJ 2018/2019 and 2019/2020. In the 2018/2019 fire season, background values (i.e. over the central South Pacific) between 0.0 and 3.0 ×10^{15} molecules cm^{-2}. The Hovmöller diagram (**Figure S7b**) shows peak $TCCH_3OH$ between 8.0 and 12.0 ×10^{15} molecules cm^{-2}, which generally co-locate with total-column carbon monoxide (TCCO) (**Figure 2b** of the main manuscript) for the 2018/2019 fire season. However, in the 2019/2020 fire season, while continental values remain similar, mean outflow $TCCH_3OH$ ranges between 3.0 and 8.0 ×10^{15} molecules cm^{-2} (**Figure S7c**), while peaking above 15.0×10^{15} molecules cm^{-2} in the Hovmöller diagram (**Figure S7d**), highlighting substantial variability. In both cases, the difference plots (**Figure S7e & f**) show large-scale enhancements in $TCCH_3OH$ (1.5-5.0 ×10^{15} molecules/cm^2 and 5.0-10.0 ×10^{15} molecules/cm^2 in the seasonal and daily differences, respectively) over the South Pacific propagating as far as South America (differences statistically significant at the 99% confidence level – see **Figure S7e**).

SM-4: Satellite Observed Methane (CH_4)

Figure S8 shows example daily IASI maps of column average CO and methane mixing ratios for 2nd and 10th January 2020. On both days, there are pronounced CO plumes substantially larger than the

background values. For CH_4 the spatial coverage is sparser due to the stringent cloud filtering and other quality control needed for reliable retrieval of methane perturbations at the ~1% level. Furthermore, CH_4 in airmasses arriving from tropical latitudes is elevated to levels comparable to that in the fire plumes. These factors make it difficult to discriminate CH_4 enhancements due to the Australian fires. Although certain CH_4 features are co-located with the main CO plumes, their spatial extent is restricted by the stringent cloud filtering, as evident in **Figure S8c & d** where the CO plume offshoot (150-180°E, 60-40°S) is not sampled in the case of CH_4. In the main manuscript (i.e. **Figure 4**) we have therefore limited attention to the daily time-series of a spatially averaged domain and the 2-week anomaly with reference to the deseasonalised, detrended decadal January mean.

SM-5: Enhancement Ratio Uncertainties

To test the robustness of the $TCCH_3OH$:TCCO enhancement ratios, we moderately perturbed some of the subjective parameters used to derive these ratios. The key parameters were time length used to study the fire period, the in-plume threshold for TCCO and the in-plume threshold for $TCCH_3OH$. The results are shown in **Table S1**, but overall we find that the derived enhancement ratios are relatively insensitive to moderate perturbations to these parameters.

References

Alvarado, M. J., et al. (2010). Nitrogen oxides and PAN in plumes from boreal fires during ARCTAS-B and their impact on ozone: an integrated analysis of aircraft and satellite observations. *Atmos. Chem. Phys.,* **10**, 9739-9760, doi:10.5194/acp-10-9739-2010.

Franco, B., et al. (2018). A General Framework for Global Retrievals of Trace Gases from IASI: Application to Methanol, Formic Acid and PAN. *J. Geophys. Res.,* **123**, 13963-13984, doi:10:1029/2018JD029633.

Logan, J. A. (1983). Nitrogen oxides in the troposphere: Global and regional budgets, *J. Geophys. Res.,* **88**, 10785– 10807, doi:10.1029/JC088iC15p10785.

Razavi, A., et al. (2011). Global distributions of methanol and formic acid retrieved for the first time from the IASI/MetOp thermal infrared sounder. *Atmos. Chem. Phys.,* **11**, 857-872, doi:10.5194/acp-11-857-2011.

Rodgers, C. D. (2000). Inverse Methods for Atmospheric Sounding: Theory and Practice, *World Sci.*, Hackensack, New Jersey, USA.

Siddans, R., Gerber, D., Bell, B. (2015). Optimal Estimation Method retrievals with IASI, AMSU and MHS measurements. Final Report, EUM/CO/13/46000001252/THH.

Siddans, R., et al. (2018). RAL Infrared Microwave Sounder (IMS) temperature, water vapour, ozone and surface spectral emissivity. *Centre for Environmental Data Analysis*, doi:10.5285/489e9b2a0abd43a491d5afdd0d97c1a4.

Veefkind, J. P., et al. (2012). TROPOMI on the ESA Sentinel-5 Precursor: A GMES mission for global observations of the atmospheric composition for climate, air quality and ozone layer applications. *Remote Sensing of Environment,* 120, 70-83. doi:10.1016/j.rse.2011.09.027.

Figures

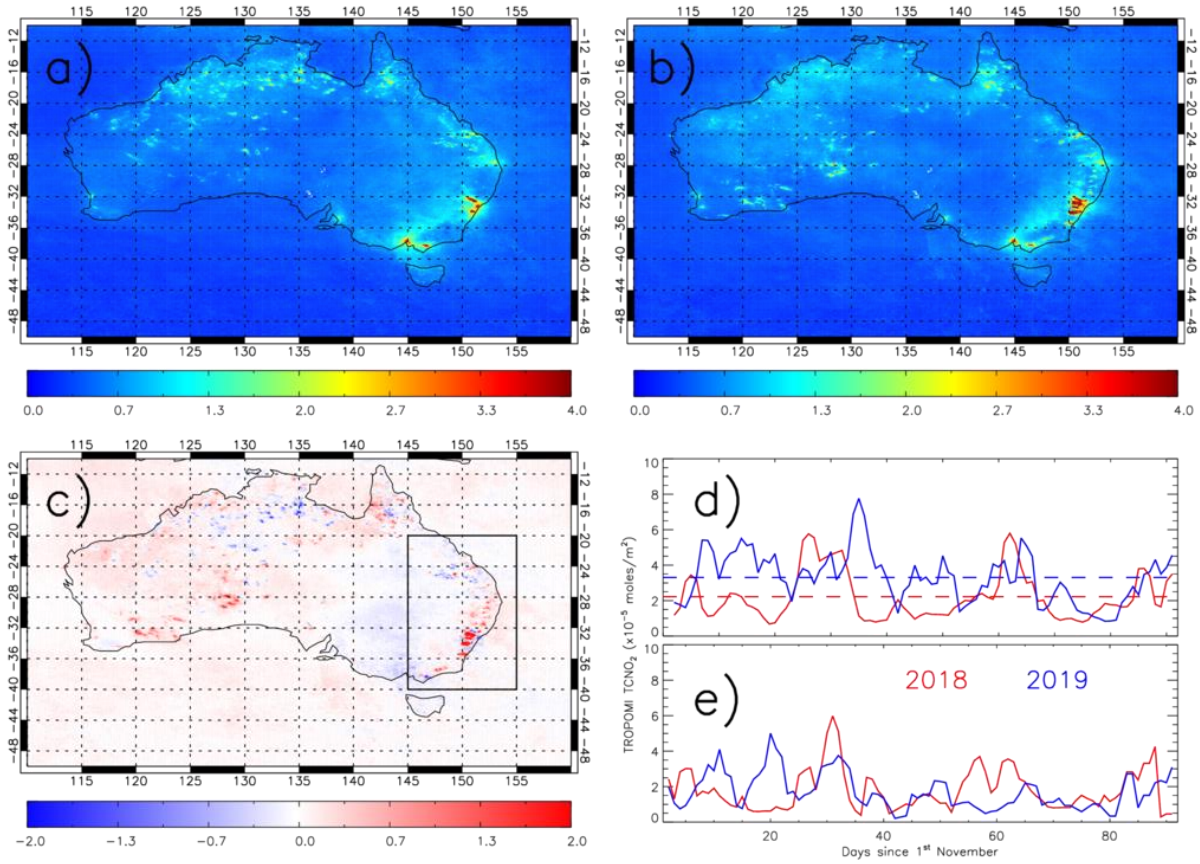

Figure S1: TROPOspheric Monitoring Instrument (TROPOMI) tropospheric column NO_2 ($TCNO_2$, 10^{15} molecules/cm^2) for a) December 2018, b) December 2019 and c) difference December 2019-2018. The black box in panel c) represents the region used in panels d) and e). Panel d) shows time series of regional NDJ $TCNO_2$ for 2018/2019 (red) and 2019/2020 (blue) weighted by regional FRP. Dashed lines represent the 3-month average. Panel e) represents regional 2018/2019 and 2019/2020 $TCNO_2$ weighted by 2019/2020 and 2018/2019 FRP, respectively.

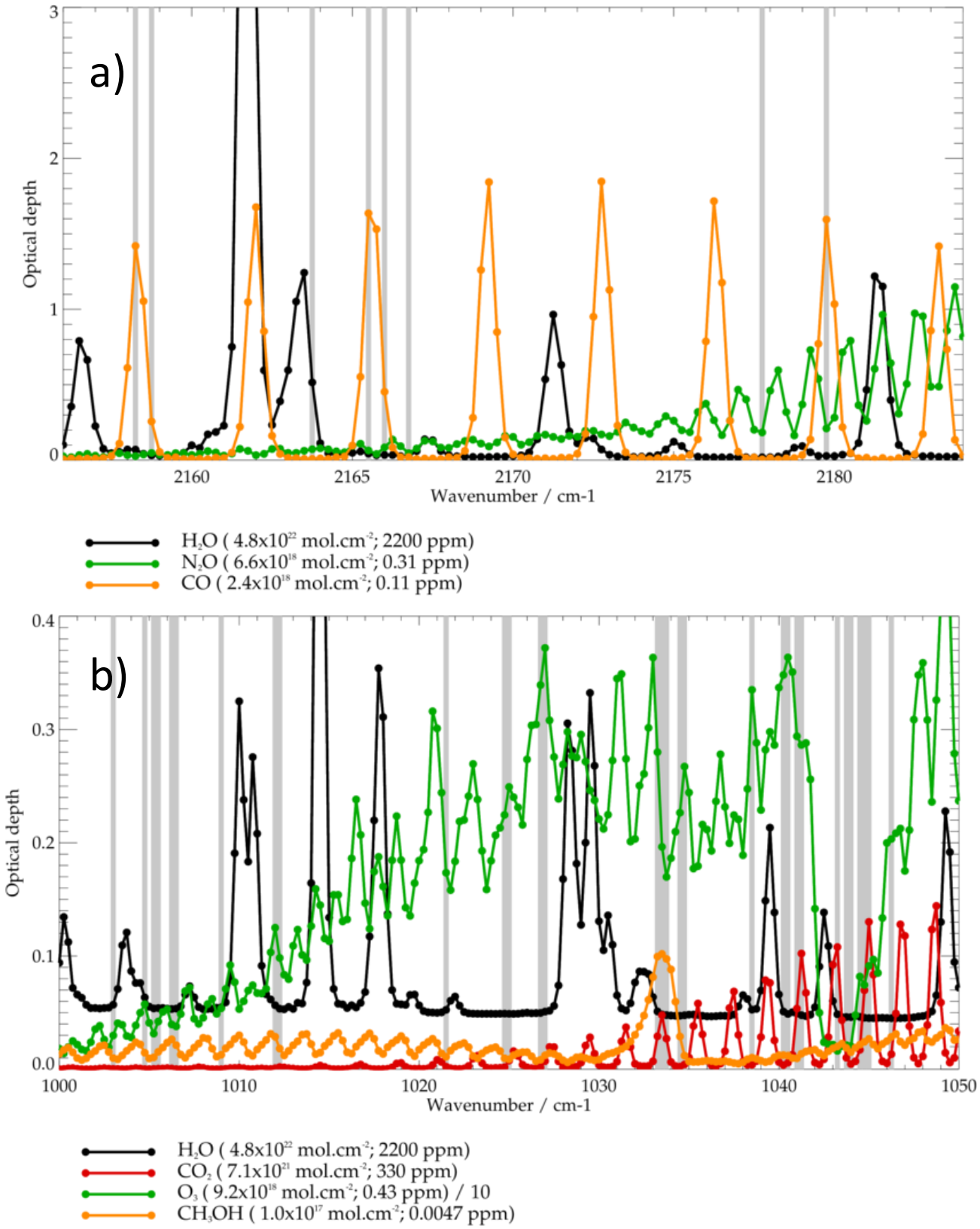

298

299 **Figure S2:** Optical depth spectra in the intervals used by the IMS extended scheme to target a) CO
300 and b) CH_3OH. The black bars are IASI spectral channels used by the retrieval scheme.

301

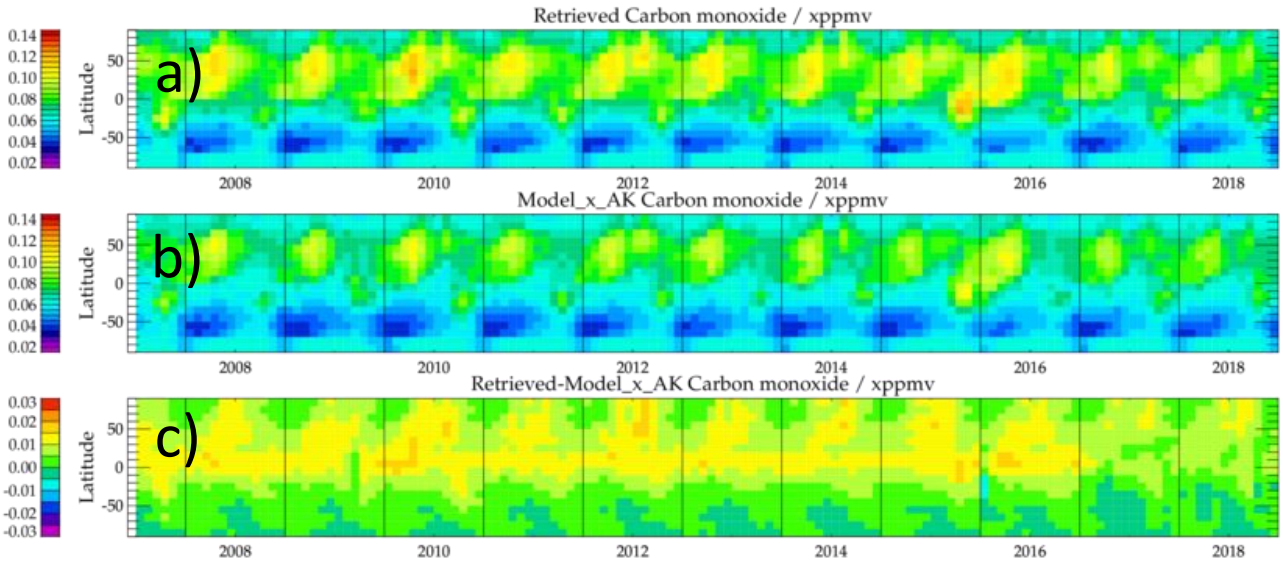

Figure S3: Column average CO volume mixing ratio retrieved from MetOp-A by the extended IMS scheme in comparison with CAMS analyses. The plots show monthly mean values in 10° latitude bins from retrievals sampled 1 day in 10. The CAMS analyses have been sampled at locations of individual MetOp soundings. Panels a) represents the retrieval, b) is the CAMS with averaging kernel and *prior* term applied (CAMS x AK) and c) is the retrieval – CAMS x AK difference.

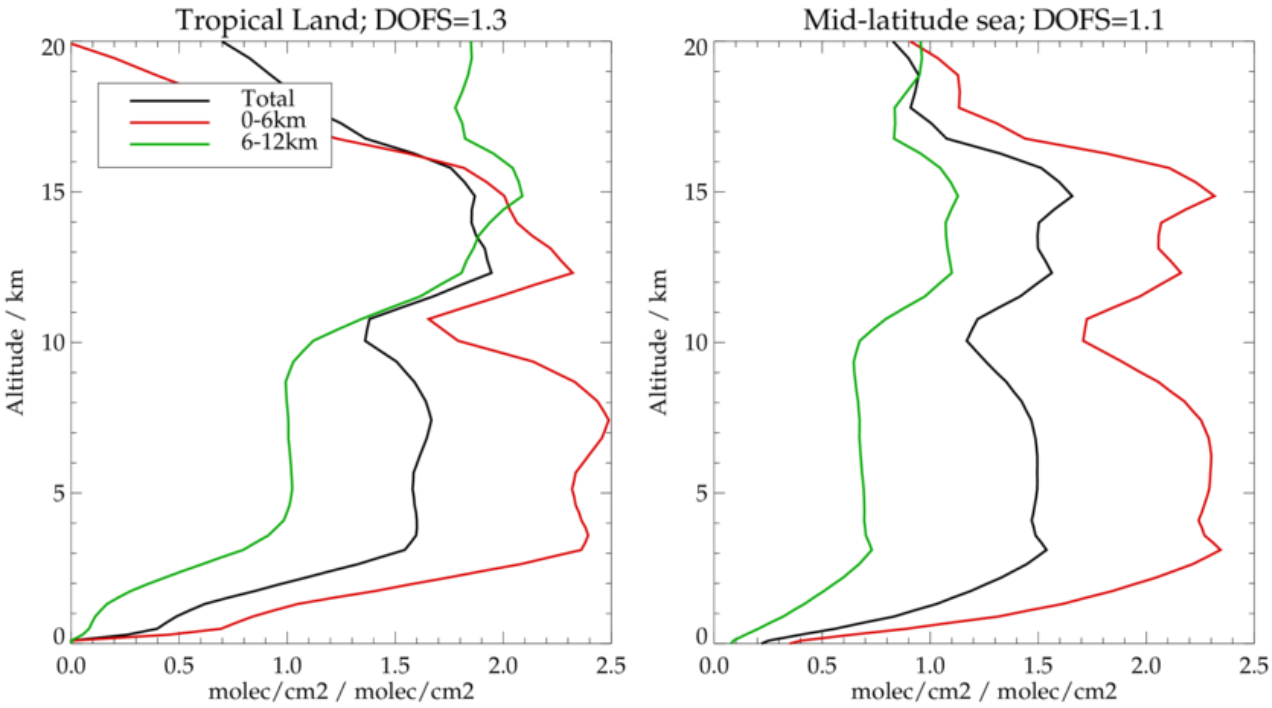

Figure S4: Vertical sensitivity for CO retrieval: averaging kernels are shown for the surface – 450 hPa (0-6 km) and 450-170 hPa (~6-12 km) layers and column average for (left) tropical land and (right) mid-latitude ocean. These are presented as the change in retrieved layer amount for a perturbation in layer amount at each vertical level. The degrees of freedom of signal are also shown above each panel, indicating the number of independent pieces of information on the vertical profile.

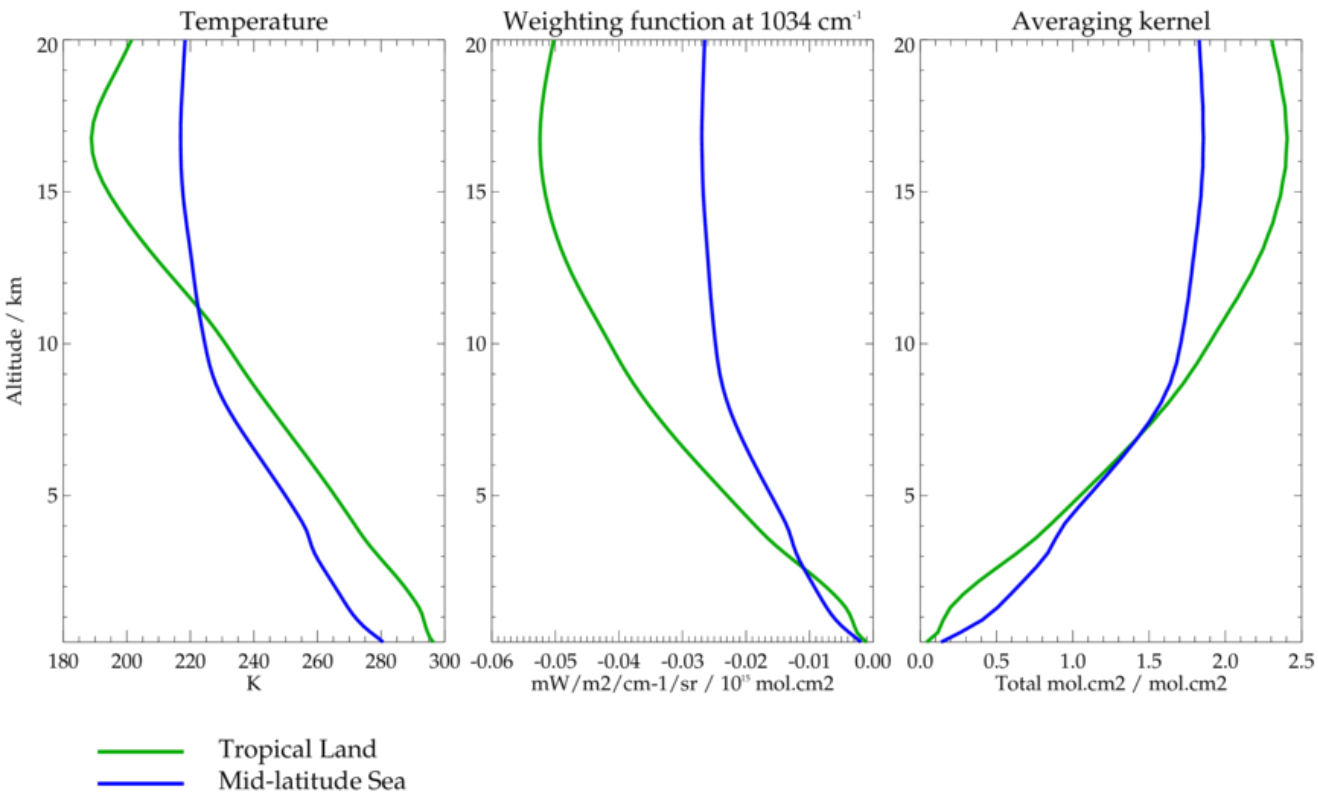

346

347 **Figure S5:** Vertical sensitivity of the CH_3OH retrieval: the figure shows temperature profiles for
348 tropical land and mid-latitude sea (left); CH_3OH weighting functions at 1034 cm-1 (centre) and
349 averaging kernels for the scale factor for the CH_3OH reference profile (constant 1 ppbv at all
350 altitudes). These are presented as the change in total column amount for a perturbation in layer
351 amount at each vertical level.

352

353

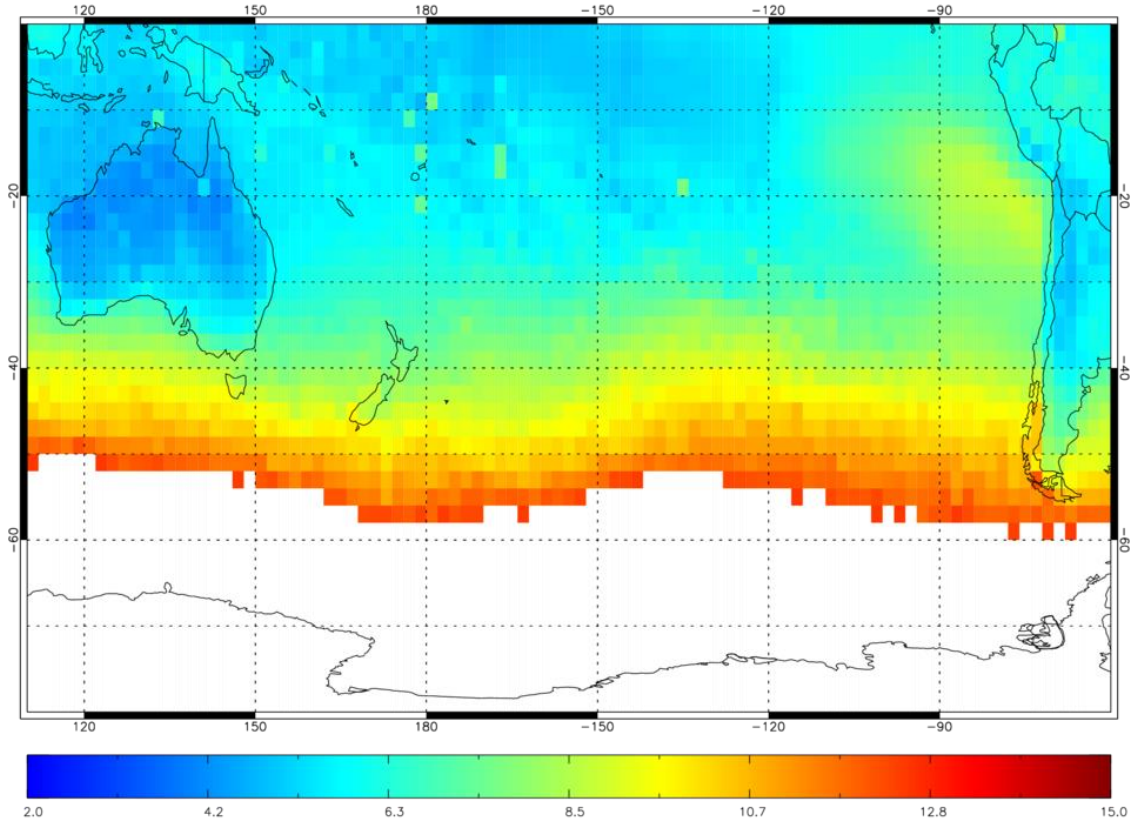

354

355 **Figure S6:** IASI $TCCH_3OH$ errors (10^{15} molecules/cm^2) for NDJ 2019/2020.

356

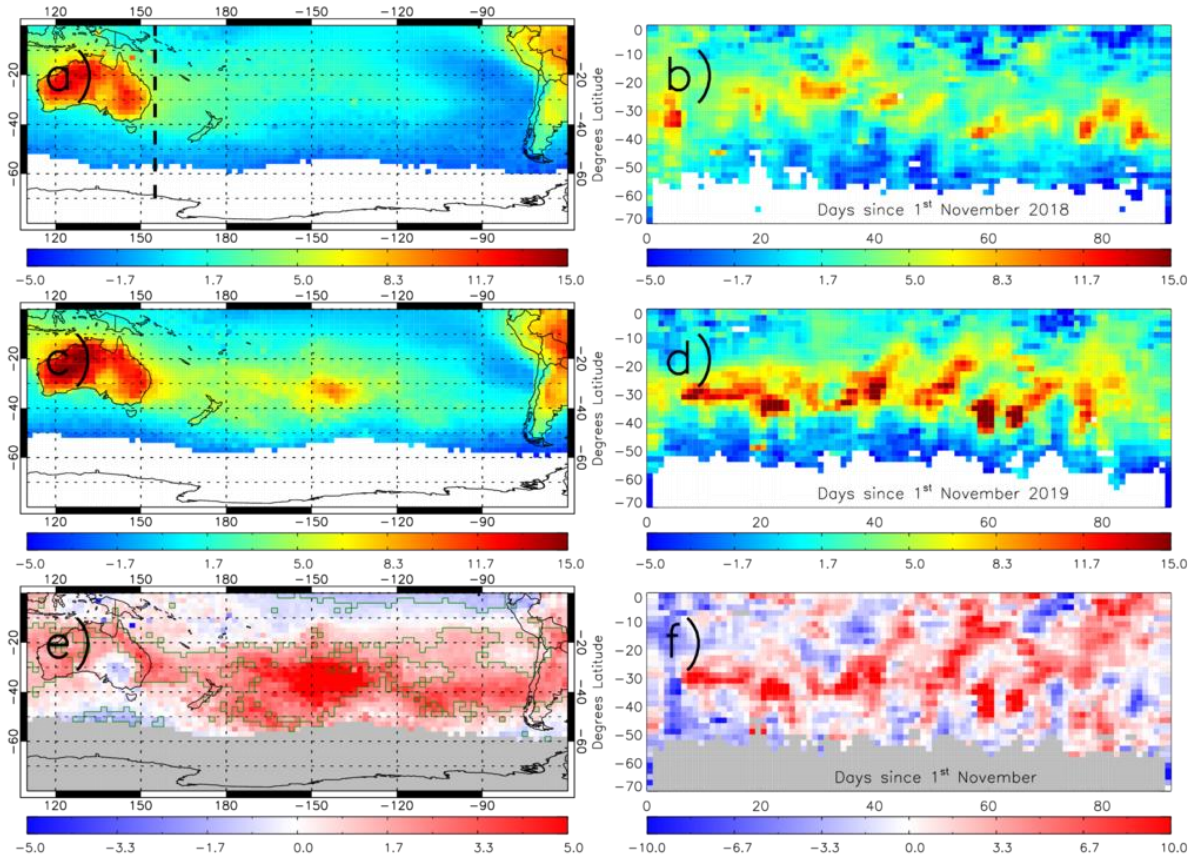

357

358 **Figure S7:** IASI NDJ total-column methanol ($TCCH_3OH$, 10^{15} molecules/cm^2) for a) 2018/2019, c)
359 2019/2020 and e) difference 2019/2020-2018/2019. Green polygon-outlined regions in panel e)
360 represent statistically significant differences between the fire seasons at the 99% confidence level
361 (CL, based on the Student t-Test) and where absolute differences are greater than 1.0×10^{15}
362 molecules/cm^2. Panels b), d) and e) represent Hovmöller diagrams of IASI $TCCH_3OH$ from November
363 – January at 155°E, between 70°S-0°S (black dashed line in panel a)), for 2018/2019, 2019/2020 and
364 the 2019/2020-2018/2019 difference, respectively. White (panels a-d) and grey (panels e & f) regions
365 represent missing data in the satellite record (i.e. average values with error terms > 15.0×10^{15}
366 molecules/cm^2).

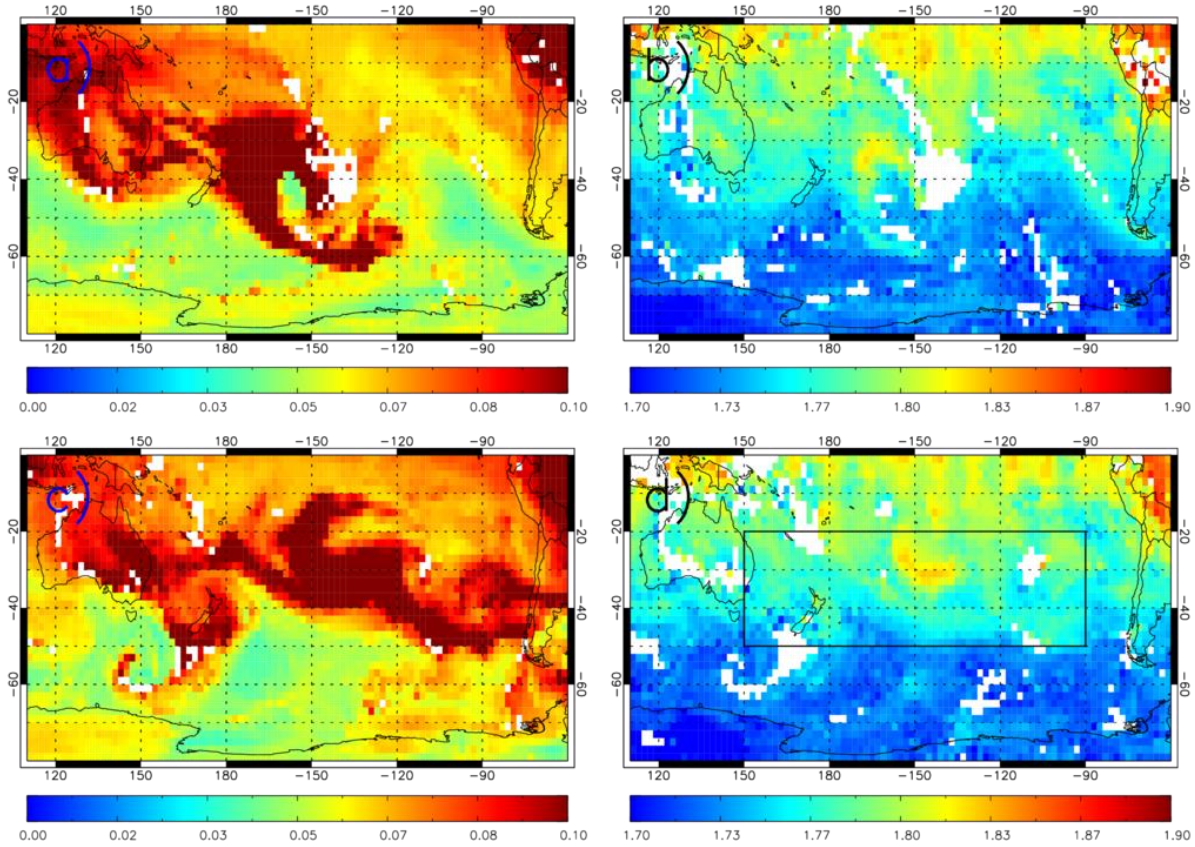

Figure S8: Daily maps of IASI column average carbon monoxide (ppmv) for 2nd and 10th January 2020 shown in panels a) & c). Corresponding column average methane (ppmv) maps are shown in panels b) and d). The black box in panel d) represents the region used to derived daily average CO and CH_4 time series in Figure 4 of the main manuscript.

Date	TCCO Threshold (molecules/cm^2)	$TCCH_3OH$ Threshold (molecules/cm^2)	Box 1	Box 2	Box 3	Box 4
1-17 Jan 2020	18 $x10^{17}$	5 $x10^{15}$	0.0036 ±5.98%	0.0059 ±3.13%	0.0091 ±1.28%	0.0081 ±1.94%
25 Dec 2019-20 Jan 2020	18 $x10^{17}$	5 $x10^{15}$	0.0050 ±4.41%	0.0053 ±3.55%	0.0096 ±1.29%	0.0083 ±2.11%
1-17 Jan 2020	16 $x10^{17}$	5 $x10^{15}$	0.0029 ±6.15%	0.0051 ±3.96%	0. 0096 ±1.29%	0.0082 ±2.07%
1-17 Jan 2020	20 $x10^{17}$	5 $x10^{15}$	0.0029 ±8.00%	0.0051 ±4.04%	0.0096 ±1.34%	0.0084 ±2.27%
1-17 Jan 2020	18 $x10^{17}$	4$x10^{15}$	0.0030 ±7.11%	0.0052 ±3.61%	0.0097 ±1.23%	0.0085 ±1.94%
1-17 Jan 2020	18 $x10^{17}$	6 $x10^{15}$	0.0028 ±7.10%	0.0049 ±4.41%	0.0094 ±1.39%	0.0081 ±2.32%

373 **Table S1**: IASI $TCCH_3OH$:TCCO enhancement ratios for the boxes in Figure 5a of main text with
374 perturbations to time period and $TCCH_3OH$:TCCO in-plume thresholds.

375